Brazilian Journal
of Chemical
Engineering

ISSN 0104-6632
Printed in Brazil
www.abeq.org.br/bjche

Vol. 33, No. 03, pp. 577 - 588, July - September, 2016
dx.doi.org/10.1590/0104-6632.20160333s20150107

ON THE SYNTHESIS OF MOLYBDENUM CARBIDE WITH COBALT ADDITION VIA GAS-SOLID REACTIONS IN A CH_4/H_2 ATMOSPHERE

C. P. B. Araujo[1*], C. P. de Souza[1], L. M. D. Maia[1], M. V. M. Souto[2] and C. M. Barbosa[3]

[1]Universidade Federal do Rio Grande do Norte, Chemical Engineering Department,
Laboratório de Materiais Nanoestruturados e Reatores Catalíticos. Av. Senador Salgado Filho,
Campus Universitário, Lagoa Nova, CEP: 59078-970, Natal - RN, Brazil.
Phone: (55) (84) 99603 7338; (55) (84) 3642 1097
*E-mail: cpbaraujo@gmail.com
E-mail: carlson@ufrnet.br; Lucas_mateus_maia@hotmail.com
[2]Universidade Federal do Rio Grande do Norte, Materials' Science and Engineering Department,
Av. Senador Salgado Filho, Campus Universitário, Lagoa Nova, CEP: 59078-970, Natal - RN, Brazil.
E-mail: Veronilda.macedo@gmail.com
[3]Instituto Federal de Educação, Ciência e Tecnologia do Rio Grande do Norte, Av. José Rodrigues
de Aquino Filho 640, RN 120, Alto de Santa Luzia, CEP: 59215-000, Nova Cruz - RN, Brazil.
E-mail: Cleonilson.mafra@ifrn.edu.br

(Submitted: February 25, 2015 ; Revised: July 10, 2015 ; Accepted: August 8, 2015)

Abstract - Due to ever more severe environmental regulations regarding SO_x, NO_x and other pollutants' emissions, there has been an interest in developing new and improved catalysts for hydroprocessing reactions. Mo_2C has been reported to display good selectivity and activity for those reactions, especially for HDS. Addition of another metal to the carbide structure may improve catalytic properties. Mo_2C with low cobalt addition (2.5 and 5%) was obtained via gas-solid reaction in a fixed bed reactor with CH_4 (5%)/H_2 atmosphere. XRD and TG/DTA analysis of the precursors were carried out in order to understand its mass loss profile, doping metal presence and phase distributions. $CoMoO_4$ as well as MoO_3 were identified after calcining doped precursors at 600 °C/180min. SEM, XRD, XRF, TOC, BET and laser granulometric analysis of the reaction products were also performed. Compositions verified by XRF and theoretical values were compatible. At 700 °C both carbide (Mo_2C) and oxide (MoO_2) phases are present, as identified in XRD analysis and observed by SEM. At 750 °C only single phase Mo_2C was verified by XRD, indicating Co dispersion on the carbide matrix. Morphology at this temperature is compatible with pure Mo_2C, though XRF indicates Co presence on the material.
Keywords: Molybdenum carbide; Cobalt; Fixed bed reactor; Solid state doping.

INTRODUCTION

Environmental regulations related to the emission of sulfur compounds constantly decrease the maximum allowed content of this element in transportation fuels (ANP, 2013). This, associated with the increase of contaminant content in crude oil worldwide, has introduced severe changes in processing of petroleum feeds, requiring more hydrogen, catalysts and heat input, which increase operational costs (Grange and Vanhaeren, 1997; Furimsky, 1998). This scenario points towards the need of developing new and improved catalysts that could substitute the traditional Ni(Co)-Mo(W)/Al_2O_3 materials currently in use.

Transition metals carbides and nitrides, especially

*To whom correspondence should be addressed
This is an extended version of the work presented at the 20th Brazilian Congress of Chemical Engineering, COBEQ-2014, Florianópolis, Brazil.

Mo, W, and Nb, find interesting applications in heterogeneous catalysis for important industrial reactions, especially for hydroprocessing, such as hydrogenation of heavy fractions and HDS (Furimsky, 2003), as well as for catalytic oxidation (Gomes, 2006), FT reaction (Griboval-Constant *et al*., 2004), methane reforming (Cheng and Huang, 2004), HDN (Al-Megren, 2005; Al-Megren, 2007) and others (Nagai and Matsuda, 2006; Vieira, 2010; Oyama, 1992a; Oyama, 1992b; Volpe and Boudart, 1985; Matar *et al*. 1988; Serge, 2003). These materials, besides having catalytic behavior similar to noble metals, also present resistance to poisoning by sulfur compounds which is an important feature of catalysts for HDT reactions (Oyama, 1992a,b).

For its use in catalysis, carbide materials are required to display a high density of active sites, small particle size and a surface area free of pollutants such as carbon or others that could impair the reaction process (Oyama, 1992a; Volpe and Boudart, 1985). These features can improve the contact between catalysts and reactants, and enhance the catalytic process (Matar *et al*., 1988; Serge, 2003).

Traditionally, carbide production derives from metallurgical processes where liquid metal is reacted with a carbon source, usually carbon black, at high temperature (1500 – 2300 °C) (Pierson, 1996; Atkins and Jones, 2006). This process, besides high temperature and energy, also demands for long residence time in order to overcome solid-state diffusion limitations (Borovinskaya *et al*., 2012).

Another route for producing monometallic carbides was developed in the 1980's at lower temperature ranges, typically by a TPR (Temperature Programmed Reaction) method using gaseous carbonaceous materials as carbon source (Oyama, 1992a; Volpe and Boudart, 1985; Lee *et al*., 1987) .

An increase of the density of active sites and, therefore, of the catalytic activity, could be attained by adding other metals to the carbide structure ideally forming systems which were similar in composition to catalysts currently in use for HDT, i.e., low Co/Mo ratio.

Bimetallic synthesis of carbide materials has been studied by several authors (Xiao *et al*., 2001; Cheng and Huang, 2004; Al-Megren, 2005; Nagai and Matsuda, 2006; Nagai *et al.* 2007; Wang *et al*., 2008), usually with compositional range above 10%Co/Mo. Most of these materials are also prepared with high carbon source content in the gas mixture: ≥20% for CH_4 (Cheng and Huang, 2004; Nagai *et al.* 2007; Izhar and Nagai, 2008; Izhar *et al*., 2009; Ma *et al*., 2014) or ≥10% for C_2H_6 (Al-Megren, 2005; Al-Megren, 2007). This can produce a higher free carbon percentage in the final product and ultimately impair the catalytic process.

This paper aims to evaluate the synthesis and characterization of molybdenum carbide with low Co addition (Co/Mo=2.5 and 5 mol%) at two temperature levels (700 and 750 °C) by using a carburizing/reducing atmosphere with low CH_4 content (5%) in order to avoid free carbon formation.

Reaction products were characterized by XRF, XRD, SEM, BET, TOC and granulometric analysis. Crystal sizes were calculated by the HWL (Halder-Wagner-Langford) equation with the integral method.

MATERIALS AND METHODS

Precursor Synthesis

Ammonium heptamolybdate (AHM) $[(NH_4)_6Mo_7O_{24}.4H_2O]$ (VETEC, Brazil, 99%) and cobalt nitrate $[Co(NO_3)_2.6H_2O]$ (CROMATO, Brazil, 98%) were manually mixed at the 2.5 and 5% molar ratios (Co/Mo) with mortar and pestle. These materials, hereafter called precursors, were subject to carbo-reduction reaction in order to synthesize the carbide materials.

TG/DTG (NETZSCH TG 209F3- Al_2O_3 crucible) analysis was carried out on precursors with 5% Co, on pure AHM, and on cobalt nitrate. All analysis' were performed in a stagnant nitrogen atmosphere with 5 °C.min^{-1} heating rate from room temperature (25 °C) to 700 °C in order to evaluate the mass loss behavior.

Precursors with 2.5 and 5% Co were calcined in a muffle furnace (EDG Inox Line 3000, Brazil) at 600 °C for 180 min for phase composition evaluation by XRD (SHIMADZU XRD- 6000, Cu Kα, operated at 30 kV and 30 mA, 2°.min^{-1}) as in the reactant atmosphere it is expected that the materials obtained via calcination are present, to some extent, as intermediates.

Carbide Synthesis

For the carbide synthesis, approximately 2 g of the precursors produced from the physical mixture of reactants, were loaded into an alumina crucible and subjected to the carbo-reduction reaction in an alumina fixed bed reactor (d_{ext}=35 mm, ℓ = 80 cm), coupled with a resistance furnace (EDG Túnel FTHI-40, Brazil). This system is presented on Figure 1, where the flow control system is also indicated.

An argon (Linde, Brazil, >99%) atmosphere was

used to purge the reactor for ~20 min before the reaction. Then the CH_4 (Linde, Brazil, >99%) and H_2 (Linde, Brazil, >99%) flow was started at a total flow rate of 15 $L.h^{-1}$ with 5% of CH_4. Heating rates of 5 $°C.min^{-1}$ and a soaking time of 180 min were used for the materials synthesized at 700 and 750 °C. Samples were tagged according to the cobalt/molybdenum ratio followed by reaction temperature (**x** % - **T** °C).

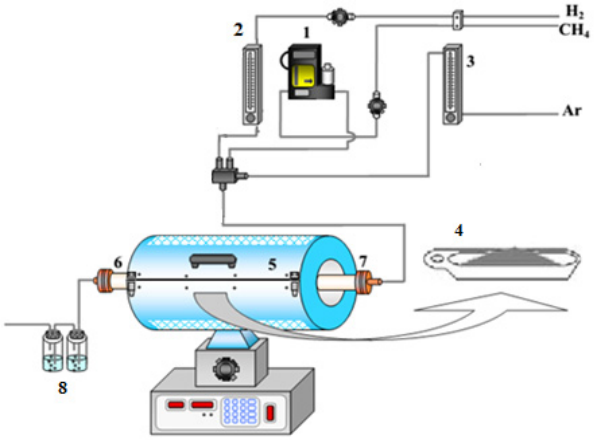

Figure 1: Fixed bed reactor coupled with resistance furnace. 1) CH_4 mass flow controller; 2) H_2 flow meter; 3) Argon flow meter; 4) Alumina crucible; 5) Resistance furnace; 6) Alumina reactor; 7) Sealing system; 8) Bubble system.

Reaction products were packed in suitable containers (closed plastic sample holders) once room temperature (25 °C) was reached. Afterwards samples were characterized by XRF (SHIMADZU EDX-720, air atmosphere), XRD, BET (Micrometrics, ASAP 2020), TOC (SHIMADZU Total Carbon Analyzer with 400ml/min O_2 flow at 900 °C) and SEM (SHIMADZU MEV SSX550 with amplifications in the range of 3, 5 and 8.10^3x).

Crystallite size was estimated by the HWL (Halder-Wagner-Langford) method with integral calculations from the mathematical profile obtained from XRD data. Laser granulometric analysis (CILAS 920 from 0,30 – 400 μm, using water as medium with no dispersing agent) were also performed.

RESULTS AND DISCUSSION

Precursors Analysis

Thermal Analysis

TG/DTA analysis was carried out on pure AHM (Figure 2), on cobalt nitrate (Figure 3), and on the precursor with 5%Co (Figure 4).

In Figure 2 four weight loss steps can be identified, accounting for a total loss of 18.97%. This result is compatible with the production of MoO_3 if $(NH_4)_6Mo_7O_{24}.4H_2O$ is considered to be the starting material. This is also in good agreement with the data published by Weinold *et al.* (2003) for AHM. All steps are accompanied by endothermic DTG signs which are relative to water and ammonia evolution of the material throughout the temperature range (RT-~450 °C).

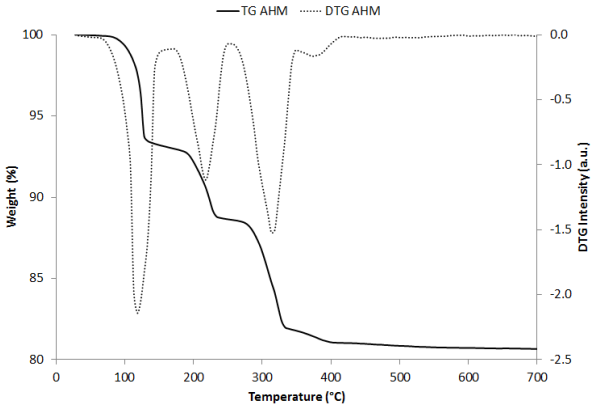

Figure 2: TG/DTA analysis for AHM.

In Figure 3 cobalt nitrate thermal decomposition is presented. A total 67.75% weight loss divided in four, almost continuous, events is verified. All events are endothermic. The first and second events, from room temperature to 200 °C, are relative to water evolution, accounting for 37.04%. The third event, which is attributed to NO_x evolution, accounts for 16.52%. The last step, attributed to chemically bonded water release, accounts for the last 17.06%. This result is in good agreement with the ones presented by other authors for the thermal decomposition of this material by a quasi-isothermal technique (Mansour, 1994; Brockner *et al.* 2007; Ehrhardt *et al.* 2005). Table 1 summarizes the results of weight loss percentage and temperature ranges of the events for the reactants and the precursor with 5% Co.

For the precursor obtained from the physical mixture of the reactants a total 19.45% weight loss was verified (Figure 4) when it was heated from room temperature to approximately 400 °C. This was attributed to H_2O, NOx, and NH_3 volatilization, as for the AHM and cobalt nitrate cases individually. Five weight loss events can be identified; those indicated with Δ refer mainly to AHM decomposition while those indicated with ■ refer to cobalt nitrate. A continuous curve with very slight slope transitions is observed, making the distinction between consecutive steps possible only by a DTG inspection in some cases.

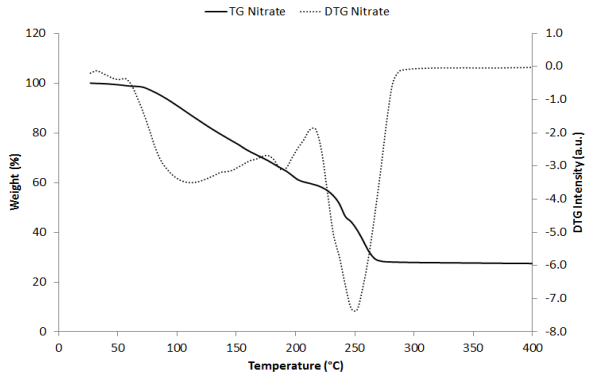

Figure 3: TG/DTG analysis for $Co(NO_3)_2.6H_2O$

Table 1: Thermal decomposition events for AHM, 5% Co percursor and cobalt nitrate.

AHM decomposition events			
Event	**Δm**	**Ts**	**Te**
1	6.92	103	148
2	4.25	178	233
3	6.57	263	333
4	0.94	333	403
Total	18.69		
5% Co Precursor decomposition events			
Event	**Δm**	**Ts**	**Te**
1	5.19	80	143
2	3.40	143	183
3	2.81	183	233
4	6.80	233	323
5	1.27	323	428
Total	19.47		
$Co(NO_3)_2.6H_2O$ decomposition events			
Event	**Δm**	**Ts**	**Te**
1	1.33	27	67
2	35.73	68	197
3	16.52	197	242
4	17.06	242	262
Total	70.64		

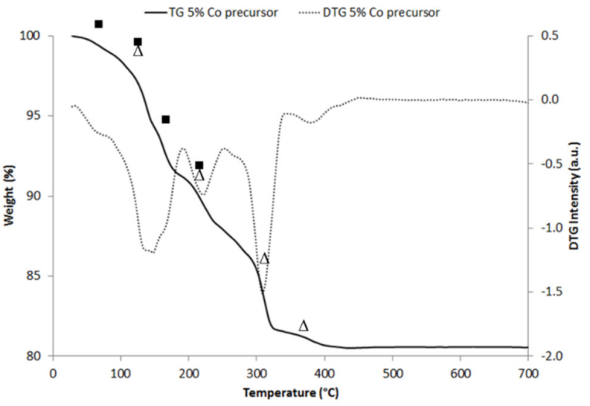

Figure 4: TG/DTA analysis for the precursor with 5%Co. ■ indicates events related to cobalt nitrate decomposition, Δ indicates events related to HMA decomposition.

Two endothermic events between room temperature and ~180 °C are relative to water volatilization, and can only be distinguished by DTG curve evaluation. In comparison with Figure 2, for the temperature range between ~100-140 °C, only one event is present and is also attributed to water evolution. In Figure 3 the same event is present but in a lower temperature range (from RT to ~70 °C.

The third decomposition step of the 5%Co precursor occurs between 180-230 °C and is attributed to NO_x elimination by nitrate groups of $Co(NO_3)_2.6H_2O$, which is in accordance with the TG data presented here in Figure 2, and accounts for a total of 2.81%. The two last events, from 230-320 °C and from 320-430 °C, are related to ammonia and water evolution and account for a total of 8.07%.

XRD Analysis

Figure 5 shows XRD patterns for precursors with 2.5 and 5% Co addition calcined at 600 °C for 180 min. Peaks marked with ■ refer to $CoMoO_4$ (ICSD: 023808) phase, whereas peaks marked with ● display a mixed contribution of both $CoMoO_4$ and

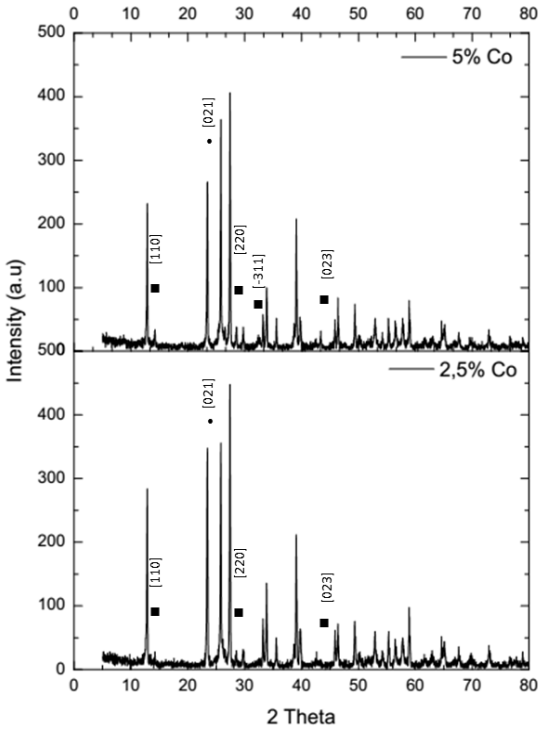

Figure 5: XRD patterns for precursors with 2.5 and 5% Co addition calcined at 600 °C for 180 min. Peaks marked with ■ refer to $CoMoO_4$ (monoclinic) phase, ● refer to mixed phase contribution: $CoMoO_4$ and MoO_3 (orthorhombic), all other peaks refer to MoO_3.

MoO_3 phases. All other peaks refer to the MoO_3 (ICSD: 076651) phase. MoO_3 phase shows orthorhombic structure, while the $CoMoO_4$ phase is monoclinic. A MoO_3 phase with this structure was identified by other authors for the thermal decomposition of AHM (Weinold *et al.* 2003), whereas $CoMoO_4$ was found in the synthesis of bimetallic Co-Mo carbides from various starting materials with Co and Mo (Cheng and Huang, 2010).

Upon decreasing the Co content, an intensity decrease in $CoMoO_4$ peaks at 14.5, 23.4, 27.3, 28.2 and 32.6 can be noted. This is more pronounced for the peak at θ=32.6°, which is no longer identified for the lower compositional level. As the Co/Mo atomic ratio increases, the $CoMoO_4$ diffraction peaks become more intense, suggesting that more $CoMoO_4$ is being formed in the bimetallic oxides (Cheng and Huang, 2010).

Reaction Products Analysis

X-Ray Fluorescence

Cobalt content in the final product was determined by X-ray Fluorescence. Table 2 shows the data obtained. It can be noted that there is agreement between expected and achieved values, showing that only relatively small loss occurred during the process. To our knowledge only a few papers, (Griboval-Constant *et al*., 2004; Al-Megren *et al*., 2005) present quantitative chemical or physical analysis for the elemental composition of the produced materials. The majority of the published articles present their phenomenological analysis based on labeling materials according to intended metal addition, as in the works of Cheng and Huang (2010), Al-Megren *et al.* (2007), Nagai and Matsuda (2006), Nagai *et al.* (2007) and Chen *et al.* (2013).

The data presented by Al-Megren *et al.* (2005) show greater deviations (~43.4%) from the intended Co/Mo ratio than the verified values presented here. Griboval-Constant *et al.* (2004), however, managed to obtain ~3% deviations in their Mo_2C supported Co catalysts.

Table 2: Co Content in the Final Product (XRF).

Sample	%wt. Co	(%)Co/Mo
2.5% - 700 °C	1.349	2.23
2.5% - 750 °C	1.359	2.24
5% - 700 °C	2.754	4.61
5% - 750 °C	2.762	4.62

X-Ray Diffraction

Figure 6 shows XRD patterns for the products of the carburization reactions at 700 and 750 °C with 2.5 and 5% Co addition. Peaks marked with ■ refer to Mo_2C (ICSD: 065701) all other peaks refer to MoO_2 (ICSD: 062210). MoO_3 is not detected in the reaction products' XRD pattern because it is reduced by H_2 forming MoO_2 before it is completely converted to carbides (Li *et al*., 1998). No cobalt-containing phases could be identified. This could be due to the low Co content added or due to the fact that this metal can be considered to be dispersed on the carbide structure. The absence of a cobalt-containing phase in the carburization product was also identified by other authors (Xiao *et al*., 2001) even when higher Co/Mo ratios were tested. The MoO_2 phase displays monoclinic structure, while Mo_2C is orthorhombic (Gomes, 2006; Wang *et al*., 2008; Li *et al*., 1998, Wang *et al*., 2006).

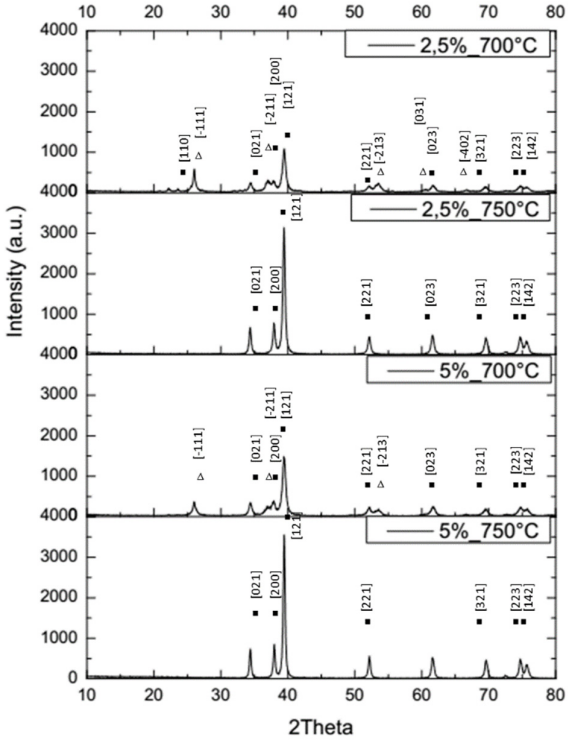

Figure 6: XRD patterns for the reaction products at 700 and 750 °C with 2.5 and 5% Co addition. Δ refers to peaks of the MoO_2 (ICSD: 062210 monoclinic) phase, and ■ refers to Mo_2C (ICSD: 065701, orthorhombic) peaks.

Other authors indicate that, because the radius of cobalt atoms is smaller than that of molybdenum atoms, the incorporation of cobalt atoms into Mo_2C

will lead to a shift to higher diffraction angle (Cheng and Huang, 2010). This phenomenon was visualized in this paper, but with a much lower intensity than those authors were able to identify since the cobalt addition was also smaller. Table 3 summarizes these angle variations for the materials where only the carbide phase was identified. This is also an indication of the presence of Co atoms in the structure of the carbide as a promoter (Cheng and Huang, 2010).

Table 3: XRD peak position deviations with increasing Co content for the materials where only the carbide phase was identified.

Peak number/ Position (2Theta)	2.5%Co 750 °C	5%Co 750 °C	Δθ
1	34.346	34.365	0.019
2	37.912	37.949	0.037
3	39.393	39.416	0.023
4	52.107	52.136	0.029
5	61.559	61.582	0.023
6	69.541	69.561	0.020
7	72.455	72.468	0.013
8	74.649	74.681	0.032
9	75.598	75.619	0.021

Crystal Size Estimates

Table 4 presents crystal size calculations for the reaction products. Calculations were carried out by applying the HWL integral method on the mathematical profile of the fitted XRD data. Correlation coefficients, as well as micro-strain estimates are also presented. For the materials produced at 700 °C, crystal sizes were 10.86 and 15.09 nm for samples with 2.5 and 5% of Co addition, respectively. At 750 °C the estimates were 30.55 and 43.25nm for samples with 2.5 and 5% of Co addition.

Even with increasing reaction temperature the crystal sizes remained nano scale. It can be noted that, with increasing temperatures, crystal size increased (~180%), which is in accordance with Avrami's theory (Avrami, 1940). The same effect can be verified upon increasing cobalt content, though with less intensity (~40%). This could be due to the fact that the Co radius is close to that of Mo and it could potentially deform the crystal network, as previously stated and verified above by XRD. Souto (2008) also verified this increase in crystal size with increase in dopant content for the synthesis of niobium carbide with copper addition. Xiao *et al.* (2001) also indicate that an increase in Co content would lead to an increase in particle size of the bimetallic Co-Mo carbide, which is in accordance with the phenomena observed here.

Table 4: Crystal size calculation results for the reaction products. The HWL integral method was used. Correlation coefficients and micro strain estimates are also presented.

Sample	HWL (nm)	ε	R^2
2.5%Co_700 °C	10.86	0.012	0.94
5%Co_700 °C	30.55	0.009	0.94
2.5%Co_750 °C	15.09	0.006	0.91
5%Co_750 °C	43.25	0.009	0.97

SEM

Scanning Electron Microscopy images are presented in Figure 7 for the reaction at 700 °C, and in Figure 8 for the carbides obtained at 750 °C. On the right side, the images refer to samples with 5%Co addition, and, on the left side, to samples with 2.5%Co addition. Highlighted regions of Figure 7(A) and (B) indicate agglomerating behavior, showing an increased tendency for agglomeration with increased Co content. In (C) and (E) the circled regions show both platelet morphology (MoO_2) and undefined morphology (Mo_2C). In Figure 8 only one type of morphology can be noted, which presents undefined shape and is attributed to the Mo_2C phase.

2.5%Co_700 °C

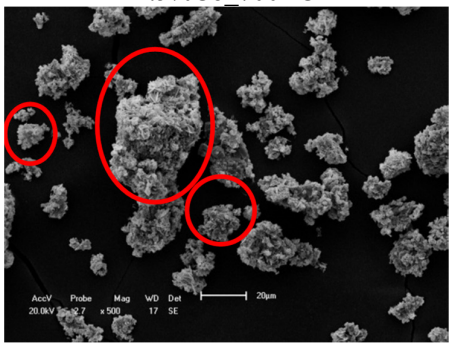

(A) 500x

5%Co_700 °C

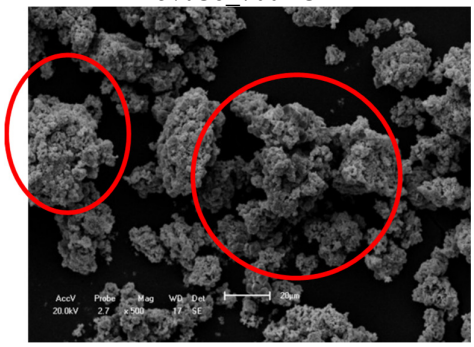

(B) 500x

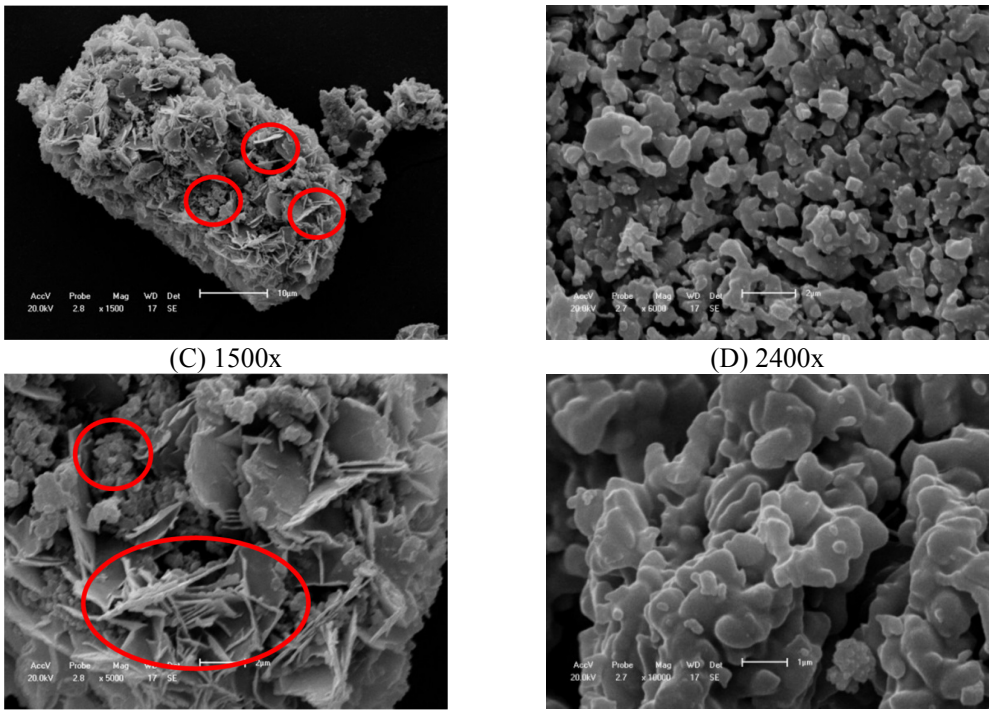

(C) 1500x (D) 2400x

(E) 10000x (F) 10000x

Figure 7: SEM images for reaction products at 700 °C. On the left side, samples with 2.5%Co, on the right side, samples with 5% Co addition. (A) and (B) with 500x magnification. (C) 1500x amplifications; platelet morphology as well as regions with undefined shape can be seen. (D) 2400x, absence of platelets morphology. (E) and (F) 10000x magnification; regions with platelets and undefined morphology.

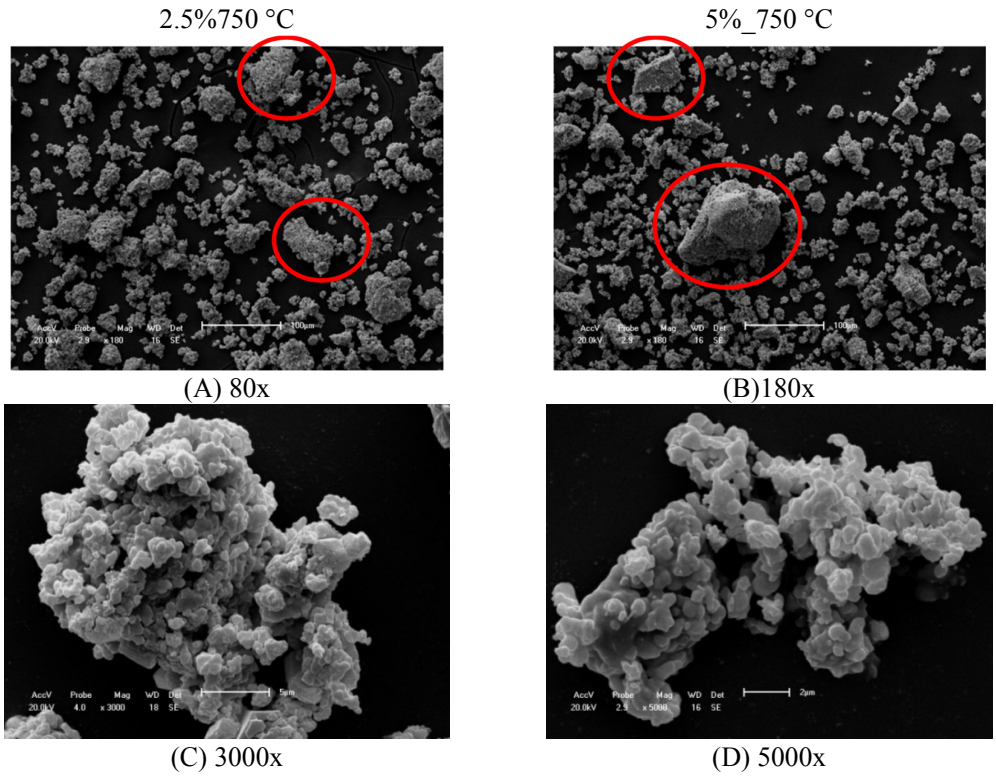

(A) 80x (B)180x

(C) 3000x (D) 5000x

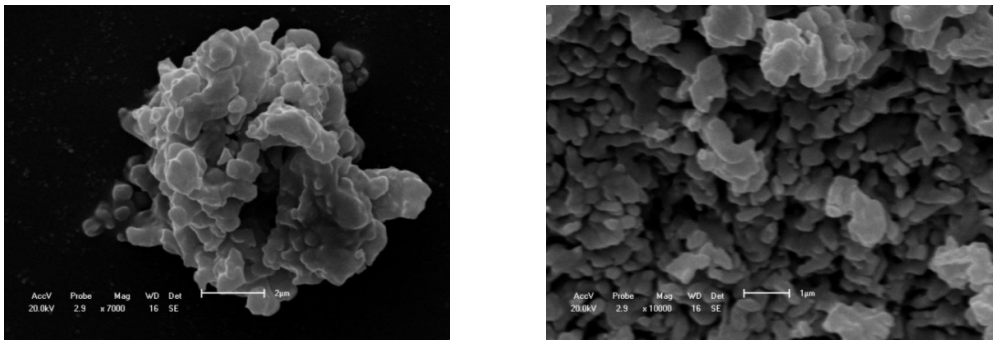

(E)7000x (F) 10000x

Figure 8: SEM images for reaction products at 750 °C. On the left side samples with 2.5% Co addition, on the right side, samples with 5%Co addition. (A) and (B) have 180x amplification. Circled regions indicate agglomerating behavior. (C) 3000x. (D) 5000x, (E) 7000x and (F) 10000x amplification. Only one morphology, with undefined shape, can be noted.

Wang *et al.* (2006) indicate, for one, that MoO_2's orthorhombic structure, which presents itself as fine platelets, can no longer identified when carburized, as it turns into isotropic particle agglomerates formed by the broken intermediate oxide particles forming the carbide material. Other papers (Gomes, 2006; Vieira, 2010; Li *et al*., 1998; Medeiros *et al*, 2001) also identify agglomerates formed by particles of unidentified shape as relative to pure carbide phase. This is in agreement with the attribution applied here.

No indication of cobalt could be found by analyzing the morphological identity of the material.

Carbon Content

Carbon content was determined by total combustion of samples at 900 °C with pure O_2. Table 5 presents the total carbon content (%wt.), as well as the carbon to metal ratio. It can be noted that only for the sample synthesized at 750 °C with lower cobalt (2.5%) content a ratio above the theoretical 0.5 value was reached. This confirms the complete conversion of oxides to carbide materials, as well as the production of a small amount of free carbon (8.9%). All other samples display ratios below the theoretical value, indicating incomplete reactions; this phenomenon is more pronounced for the 700 °C samples, in accordance with the XRD data presented here. For the material with 5% Co produced at 750 °C, approximately 86% conversion was obtained. This high conversion could explain the difference between this data and the phases identified by XRD, as the majority of the material consists of carbide phase.

Griboval-Constant *et al.* (2004) produced molybdenum carbide with low ruthenium or cobalt addition, at 700 °C and 10%CH_4–H_2 with a 6 h soaking time and obtained carbon contents of 4.5 and 5.2% (wt.) for the doped materials. This is over 30% of the maximum carbon content verified here. A possible explanation would be the longer soaking time applied coupled with higher methane content in the reactant mixture.

Al-Megren *et al*., (2005) also evaluated the carbon content of their carbide materials and attained 6.1% wt. before the HDN reaction. This result is 78% above the highest value achieved in this paper. This higher carbon percentage is probably due to the carbon source used (C_2H_6) and its amount in the total mixture (10%).

As can be noted, the use of methane as a carbon source and shorter soaking times managed to reduce the free carbon content in the final product in comparison to these authors, though the synthesis of pure carbide materials needed a finer flow/synthesis control.

Table 5: Carbon content analysis of the reaction products.

Sample	Total carbon content (%wt.)	C/Metal
2.5%Co_700 °C	1.84	0.31
2.5%Co_750 °C	3.45	0.59
5%Co_700 °C	2.17	0.37
5%Co_750 °C	2.71	0.46

BET

Superficial area was determined by BET analysis of the carburized materials and is presented in Table 6. Low values were obtained, as these materials were not passivized. No tendency regarding the change of parameters could be noted.

These surface areas values are compatible with the work of Griboval-Constant *et al.* (2004), who also verified (for molybdenum carbide with Ru or Co addition) superficial areas in the range of 3-9 $m^2.g^{-1}$, with the highest area being relative to pure Mo_2C (9.2 $m^2.g^{-1}$). Al-Megren *et al.* (2005) also managed to obtain superficial areas close to 20 m^2g^{-1} for bimetallic cobalt molybdenum carbide with a Co/Mo ratio of 0.67 produced by TPR with ethane at 10%.

Xiao *et al.* (2001), however, by using an elaborate series of steps (mixture, dissolution in organic solvent, evaporation, calcination, pelletization and carbo-reduction reaction) were able to achieve higher superficial areas 15.5-39.6 m^2g^{-1}. One would still need to provide an evaluation of the cost of these operations vs. superficial area increase, as these values are close to the ones obtained here and required much more processing.

Table 6: BET evaluation of the reaction products.

Sample	Surface area (m^2/g)	Pore size (cm^3/g)
2.5%Co_700 °C	16.68	0.040
2.5%Co_750 °C	24.39	0.040
5%Co_700 °C	16.76	0.030
5%Co_750 °C	17.88	0.025

Laser Granulometric Analysis

Laser granulometric analysis was carried out on the carburized materials to identify if the tendency noted in SEM analysis could be extended to the entire material. Figure 9 shows the distributions obtained. Table 7 provides the data for average agglomerate diameter, and the diameter obtained when the smallest 10, 50 and 90% fractions of the distribution were considered.

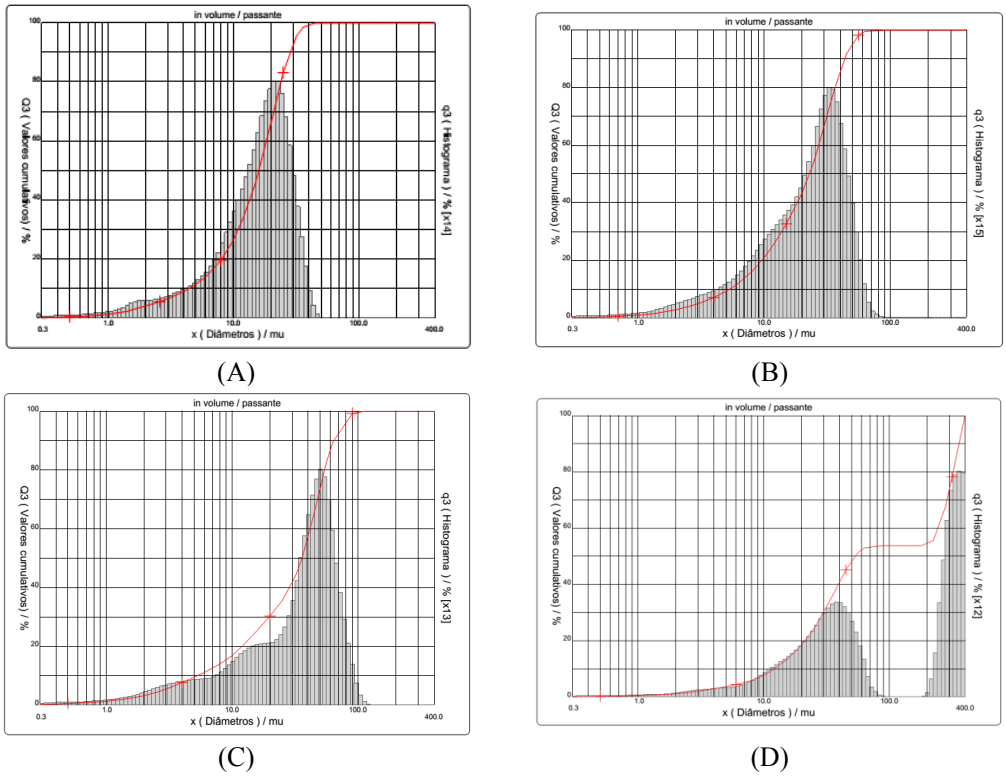

Figure 9: Results for the laser granulometric analysis of the reaction products. (A) at 700 °C with 2.5%Co and $d_{average}$= 14.94 µm. (B) at 750 °C with 2.5% Co and $d_{average}$=26.34 µm. (C) at 750 °C with 5% Co and $d_{average}$=39.85 µm. (D) at 750 °C with 5%Co and $d_{average}$=168.45 µm

Table 7: Agglomerates size distribution for the reaction products. The cut sizes for 10, 50 and 90% of the particles are presented, as well as the average for the entire sample.

D (μm)	2.5% Co_700 °C	2.5% Co_750 °C	5% Co_700 °C	5% Co_750 °C
10%	3.98	5.97	6.64	12.65
50%	14.7	24.55	38.55	134.48
90%	25.98	48.64	73.4	359.30
Average	14.94	26.34	39.85	168.45

This analysis was able to quantify the agglomerate size distribution and indicated that an increase in cobalt content led to the formation of larger agglomerates, for the same reaction temperature. If the temperature is increased there was also an increase in the agglomerate sizes. This could be explained on the basis of the carbide formation process, as intermediate oxide particles are broken to form the carbide phase, which then has a smaller particle size and, therefore, is more prone to agglomerate due to electrostatic forces. No other paper, to our knowledge, has presented this kind of analysis of their carbide materials. We find that this is important information for future process scale-up as the agglomerating behavior of the powder has a direct effect on the final use of the materials and can be altered, to some extent, by reactor parameters such as type of reactor, gas flow and precursor loading.

CONCLUSIONS

From the method proposed here it was possible to obtain MoO_3 and $CoMoO_4$ phases by providing heat treatment to the precursor produced from the physical mixture of cobalt nitrate and AHM. The presence of $CoMoO_4$ at this stage is an indicative of the intimate contact of Co and Mo atoms in the precursor.

Precursors with 2.5% cobalt addition were able to produce single phase molybdenum carbide at 750 °C with a 180min soaking time with low free carbon content (~8.9%). For the powder produced at this temperature with 5% Co, TOC analysis indicated that an 86% conversion was achieved, which suggests that probably longer soaking times would be needed to form pure Mo_2C with this Co content.

All materials produced at 700 °C were composed of a mixture of molybdenum oxide and carbide, indicating incomplete reactions, which were identified by XRD and confirmed by TOC and SEM images. This could be due to the low methane composition used in the gas mixture.

It was found that cobalt addition produced a shift in diffraction angles of the molybdenum carbide phase, which indicates its presence in the carbide structure, as no cobalt-containing phases were identified by XRD for the reaction products. XRF data also confirmed the Co presence in all materials, which, coupled with the XRD verification, suggests the actual presence of this metal in the structure as a promoter.

Co addition also altered the agglomerating behavior of the carbide materials making them more prone to form larger agglomerates, as electrostatic forces are changed with increasing cobalt content.

ACKNOWLEDGEMENTS

We thank CNPq, UFRN, PPGCEM and PPGEQ for all the support in developing the data and research.

SYMBOLS AND UNITS

AHM	Ammonium Heptamolybdate
d	Crystal size (nm)
θ	Diffraction angle (°)
HDS	Hydrodesulphurization
HDT	Hydrotreatment
TOC	Total organic carbon
XRD	X Ray Diffraction
XRF	X Ray Fluorescence
HWL	Halder-Wagner-Langford

REFERENCES

ANP, Agência Nacional do Petróleo, Gás Natural e Biocombustíveis. RESOLUÇÃO ANP Nº 50- DOU 24.12.2013. ANP. [S.l.]. (2013). (In Portuguese).

Al-Megren, H. A., Xiao, T., Gonzalez-Cortes, S. L., Al-Khowaiter, S. H., Green, M. L. H., Comparison of bulk CoMo bimetallic carbide, oxide, nitride and sulfide catalysts for pyridine hydrodenitrogenation. Journal of Molecular Catalysis, A: Chemical, 225, p. 143-148 (2005).

Al-Megren, H. A., Gonzalez-Cortes, S. L., Xiao, T., Green, M. L. H., A comparative study of the catalytic performance of Co-Mo and Co(Ni)-W carbide catalysts in the hydrodenitrogenation (HDN) reaction of pyridine. Applied Catalysis, A: General, 329, p. 36-45 (2007).

Atkins, P., Jones, L., Princípios de Quimica - Questionando a Vida Moderna e o Meio Ambiente. 3ª, Ed. Porto Alegre: Bookman (2006). (In Portuguese).

Avrami, M., Kinetics of phase change. II Transformation-time relations for random distribution of nuclei. Journal of Chemical Physics, 8, p. 212-224 (1940).

Borovinskaya, I., Ignatieva, T., Vershinnikov, V., Nanda Kumar, A. K., Kurokawa, K., Madej, M., Pędzich, Z., Twardowski, P., Wojciechowski, S., Fan, Y., Tungsten Carbide – Processing and Applications. 1st, Ed. [S.l.]: INTECH (2012).

Brockner, W., Erhardt, C., Gjikaj, M., Thermal decomposition of nickel nitrate hexahydrate, $Ni(NO_3)_2.6H_2O$, in comparison to $Co(NO_3)_2.6H_2O$ and $Ca(NO_3)_3.4H_2O$. Thermochimica Acta, 456, p. 64-68 (2007).

Chen, W., Muckerman, J. T., Fujita, E., Recent developments in transition metal carbides and nitrides as hydrogen evolution electrocatalysts. Chem. Comm., 49, p. 8896-8909 (2013).

Cheng, J., Huang, W., Effect of cobalt (nickel) content on the catalytic performance of molybdenum carbides in dry methane reforming. Fuel Processing Technology, 91, p. 185-193 (2010).

Ehrhardt, C., Gjikaj, M., Brockner, W., Thermal decomposition of cobalt nitrato compounds: Preparation of anhydrous cobalt(II)nitrate and its characterisation by Infrared and Raman spectra. Thermochimica Acta, 432, p. 36-40 (2005).

Furimsky, E., Review: Selection of catalysts and reactors for hydroprocessing. Applied Catalysis, A: General, 171, p. 177-206 (1998).

Furimsky, E., Review: Metal carbides and nitrides as potencial catalysts for hydroprocessing. Applied Catalysis A: General, 240, p. 1-28 (2003).

Grange, P., Vanhaeren, X., Hidrotreating catalysts, an old story with new challenges. Catalysis Today, 36, p. 375-391 (1997).

Griboval-Constant, A., Giraudon, J. M., Leclercq, G., Leclercq, L., Catalytic behaviour of cobalt or ruthenium sopported molybdenum carbide catalyst for FT reaction. Applied Catalysis, A: General, 260, p. 35-45 (2004).

Gomes, K. K. P., Sintese e caracterização do carbeto de molibdênio nanoestruturado para fins catalíticos na reação de oxidação parcial do metano. Universidade Federal do Rio Grande do Norte. Natal. Masters Thesis (2006). (In Portuguese).

Izhar, S., Nagai, M., Cobalt molybdenum carbides as anode electrocatalyst for proton exchange membrane fuel cell. Journal of Power Sources, 182, p. 52-60 (2008).

Izhar, S., Nagai, M., Yoshida, M., Characterization and performances of cobalt–tungsten and molybdenum-tungsten carbides as anode catalysts for PEFC. Electrochimica Acta, 54, p. 1255-1262 (2009).

Lee, J. S., Oyama, S. T., Boudart, M., Molybdenum carbide catalysts: I. Synthesis of unsupported powders. Journal of Catalysis, 106, p. 125-133 (1987).

Li, S., Kim, W. B., Lee, J. S., Effect of the reactive gas on the solid-state transformation of molybdenum trioxides to carbides and nitrides. Chem. Mater., 10, p. 1853-1862 (1998).

Ma, Y., Guan, G., Shi, C., Zhuc, A., Hao, X., Wang, Z., Kusakabe, K., Abudula, A., Low-temperature steam reforming of methanol to produce hydrogen over various metal-doped molybdenum carbide catalysts. International Journal of Hydrogen Energy, 39, p. 258-266 (2014).

Mansour, S. A. A., Spectrotherrnal studies on the decomposition course of cobalt oxysalts. Part II Cobalt nitrate hexahydrate. Materials Chemistry and Physics, 36, p. 317-325 (1994).

Matar, S., Mirbach, M. J., Tayim, H. A., Catalysis in Petrochemical Processes. Dordrecht/Boston/London: Kluwer Academic Publishers. DOI: 10.1007/978-94-009-1177-2 (1988).

Medeiros, F. F. P., De Oliveira, S. A., De Souza, C. P., Da Silva, A. G. P., Gomes, U. U., De Sousa, J. F., Synthesis of tungsten carbide through gas – solid reaction at low temperatures. Materials Science and Engineering, A, 315, p. 58-62 (2001)

Nagai, M., Matsuda, K., Low-temperature water-gas shift reaction over cobalt-molybdenum carbide catalyst. Journal of Catalysis, 238, p. 489-496 (2006).

Nagai, M., Izhar, S., Kanesugi, H., Tominaga, H., Cobalt molybdenum carbides: Surface properties and reactivity for methane decomposition. Applied Catalysis A: General, 317, p. 82-90 (2007).

Oyama, S. T., Preparation and catalytic properties of transition metal carbides and nitrides. Catalysis Today, 15, p. 179-200 (1992a).

Oyama, S. T., Crystal structure and chemical reactivity of transition metal carbides and nitrides. Journal of Solid State Chemistry, 96, p. 442-445 (1992b).

Pierson, H. O., Handbook of Refractory Carbides and Nitrides: Properties, Characteristics, Processing and Applications. Albuquerque, New Mexico (1996).

Serge, R., Thermal and Catalytic Processes in Petroleum Refining. Nova York, Marcel Dekker (2003).

Souto, M. V. M., Síntese e caracterização de $CuNb_2O_6$ e CuNbC através de reação sólido-sólido e gás-sólido a baixa temperatura. Master's Thesis, Universidade Federal do Rio Grande do Norte, Natal (2013). (In Portuguese).

Vieira, J. R. G., Avaliação de catalisadores a base de carbeto e nitreto de molibdênio na obtenção de lactitol via hidrogenação da lactose. Doctor's Thesis, Universidade Federal do Rio Grande do Norte, Natal (2010). (In Portuguese).

Volpe, L., Boudart, M., Compounds of molybdenum and tungsten with high specific surface area: II Carbide. Journal of Solid State Chemistry, 59, p. 348-356 (1985).

Wang, X.-H., Hao, H. L., Zhang, M. H., Li, W., Tao, K. Y., Synthesis and characterization of molybdenum carbides using propane as carbon source. Solid State Chemistry, 179, p. 538-543 (2006).

Wang, X.-H., Zhang, M. H., Li, W., Tao, K. Y., Synthesis and characterization of cobalt-molybdenum bimetallic carbides catalysts. Catalysis Today, 131, p. 111-117 (2008).

Weinold, J., Jentoft, R. E., Ressler, T., Structural investigation of the thermal decomposition of ammonium heptamolybdate by in situ XAFS and XRD. European Journal of Inorganic Chemistry, 6, p. 1058-1071 (2003).

Xiao, T.-C.,York, A. P. E., Al-Megren, H., Williams, C. V., Wang, H. T., Green, M. L. H., Preparation and characterisation of bimetallic cobalt and molybdenum carbides. Journal of Catalysis, 202, p. 100-109 (2001).